Effect of partial exfoliation in carbon dioxide adsorption-desorption properties of carbon nanotubes

P. Tamilarasan and S. Ramaprabhu

Citation: Journal of Applied Physics **116**, 124314 (2014); doi: 10.1063/1.4896669
View online: http://dx.doi.org/10.1063/1.4896669
View Table of Contents: http://scitation.aip.org/content/aip/journal/jap/116/12?ver=pdfcov
Published by the AIP Publishing

Effect of partial exfoliation in carbon dioxide adsorption-desorption properties of carbon nanotubes

P. Tamilarasan and S. Ramaprabhu[a)]
Alternative Energy and Nanotechnology Laboratory (AENL), Nano Functional Materials Technology Centre (NFMTC), Department of Physics, Indian Institute of Technology Madras (IITM), Chennai, India

(Received 29 August 2014; accepted 17 September 2014; published online 30 September 2014)

In this study, we have experimentally studied the effect of partial exfoliation in low-pressure (<100 kPa) carbon dioxide adsorption and desorption behavior of multiwalled carbon nanotubes (MWNTs). MWNTs were partially exfoliated by controlled oxidation followed by hydrogen assisted low temperature exfoliation method. The adsorption capacity of partially exfoliated MWNTs (PEMWNTs) is 3.4 times that of MWNTs. Adsorption-desorption isotherms of MWNTs are unique, which shows trapping behavior. The desorption behavior in association with isothermal adsorbate retention of MWNTs and PEMWNTs suggests possible CO_2 trapping inside the tubes and at interstitials. It is found that the CO_2 adsorbed PEMWNTs system has higher molecular orbital energy than CO_2 adsorbed MWNTs system. Areal adsorption capacity analysis suggests the significant influence of surface functional groups on adsorption capacity. Adsorption isosteres of both adsorbents follow the Arrhenius relation stating the temperature dependent adsorption rate. The isosteric heats and change in entropy of adsorption have been determined at multiple adsorbed amounts from the corresponding adsorption isosteres. © *2014 AIP Publishing LLC*.
[http://dx.doi.org/10.1063/1.4896669]

I. INTRODUCTION

The development of solid-state adsorbents for carbon dioxide capture has attained significant importance as the captured CO_2 can be used for industrial needs. Several solid state adsorbents, including zeolites, metal chalcogenide nanostructures, metal organic frameworks, polymers, carbon nanomaterials (CNMs), and their hybrids have been extensively developed as adsorbents for CO_2 capture.[1–5] Among them, carbon nanostructures are well known as adsorbents due to their low density, high surface area, and porosity along with good chemical stability. The advantages of CNMs include the fast adsorption/desorption, which render them as suitable adsorbent for gas adsorption related applications.[6] Moreover, the ease of surface covalent functionalization with wide variety of functionalities, such as hydroxyl, carboxyl, epoxy, and carbonyl, facilitates tuning the adsorption properties of CNMs. In addition, CNMs anchor the noncovalent functionalities, such as metal/metal-chalcogenide nanostructures, ionic liquids, and polymers, which produce efficient adsorbents for CO_2 capture at high pressures.[7–9]

The low pressure (<10 Torr) carbon dioxide adsorption analysis on graphite, graphitized carbon, and natural diamond has been reported by Deitz.[10] Recently, Guo *et al*. have briefly studied the CO_2 adsorption properties of activated carbon and derived the thermodynamic parameters at sub-ambient pressures.[11] Carbon nanotubes have potential applications in gas adsorption, due to their 1D structure, low density, high surface area, porosity, and ease of functionalization. The carbon dioxide adsorption properties of 1D multiwalled carbon nanotubes (MWNTs) are studied and their thermodynamic parameters are determined.[12] The interesting features of carbon nanotubes in gas adsorption applications lead to the theoretical studies of various aspects of CO_2 adsorption on them.[13] The structure of adsorbed CO_2 along with its thermodynamic parameters has been determined, where it is reported that CO_2 molecules find grooves as suitable sites for accommodation.[14] The interstitial space of carbon nanotubes bundles can be viewed as grooves, which are stronger adsorption sites.[15]

The binary mixture of carbon nanotubes and graphene (a 1D, 2D mixture) is expected to have enhanced adsorption properties due to the prevention of face-to-face agglomeration of graphene.[16,17] Moreover, it makes large amount of groove-like adsorption sites to anchor more amount of CO_2 molecules.

It is anticipated that the surface area, porosity, and affinity towards adsorbate are the major factors determining the adsorption properties. In addition, surface chemistry of carbon nanomaterials strongly affects the CO_2 adsorption capacity. The effect of surface modification of activated carbon has been extensively studied.[18] Kalili *et al*. have studied the effect of *carboxylation* on CO_2 adsorption properties of MWNTs and activated carbon.[19] In general, functional moieties and defects improve the CO_2 adsorption capacity of carbon nanomaterials.

The specific surface area (SSA) of MWNTs can be improved by unraveling few of the outer layers.[20,21] Recently, we have synthesized partially exfoliated MWNTs (PEMWNTs) by controlled unraveling of outer layers and realized their applications in supercapacitor.[22] In this context, a comparative study on CO_2 adsorption properties of MWNTs (1D) and PEMWNTs (1D + 2D) is essential to understand the influence of major structural changes, which will explore their additional application.

[a)]Email: ramp@iitm.ac.in

In the present study, we have investigated the low-pressure CO_2 adsorption properties of MWNTs (1D) and PEMWNTs (1D + 2D) at multiple temperatures. The thermodynamic parameters of adsorption have been determined. To the best of our knowledge, this is the first investigation on the influence of partial exfoliation on CO_2 adsorption properties of MWNTs.

II. EXPERIMENTAL SECTION

A. Material synthesis

Carbon nanotubes: MWNTs were synthesized using catalytic chemical vapor deposition (CCVD) technique, where Ni based AB_3 alloy hydride was used as catalyst. First, alloy catalyst was decrepitated by repeated hydrogen adsorption-desorption cycles. MWNTs were grown on the surface of catalyst by pyrolysis of acetylene (carbon precursor) at 973 K in argon atmosphere in a tubular furnace. Air oxidation and acid treatment were employed to remove amorphous carbon and catalytic impurities from the as grown MWNTs, respectively.[23]

PEMWNTs: PEMWNTs were synthesized by a similar route followed in our previous study.[22] Briefly, MWNTs were oxidized by water-free mixture of concentrated sulphuric acid, sodium nitrate, and potassium permanganate.[24] In this method, oxidation of MWNTs has been controlled by reducing the amount of $KMNO_4$ (1.5 g per gram of graphite, unlike conventional Hummers' method), while the ratio of H_2SO_4 and $NaNO_3$ is unchanged. This helps to restrict oxidation to a few outer layers of MWNTs and results partially oxidized MWNTs (POMWNTs). At least 60%–70% weight gain has been observed upon oxidation, due to the possible inclusion of oxygen containing functional groups into carbon layers. Here, $KMNO_4$ unzips the outer layers of MWNTs and makes it possible to insert functional groups into the inter-layer distance.[25]

In the following step, hydrogen-assisted low-temperature exfoliation of POMWNTs results in PEMWNTs. Briefly, a tubular furnace was charged with POMWNTs (200 mg) and the temperature is raised to 473 K in hydrogen atmosphere. Functional groups present at the oxidized walls react vigorously with hydrogen. Rapid removal of functional groups results in exfoliation of oxidized outer layers and unravels them to produce PEMWNTs.[26]

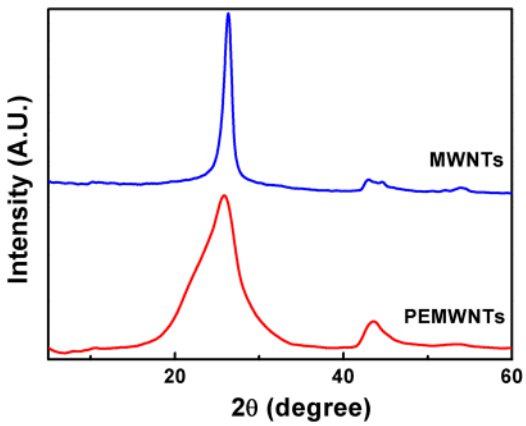

FIG. 1. X-ray diffraction pattern of MWNTs and PEMWNTs.

B. Characterization techniques

X'Pert Pro PANalytical powder X-ray diffractometer has been employed for structural analysis. The surface morphology of carbon nanomaterials was determined by transmission electron microscopy (TEM) using Technai G-20. A Perkin-Elmer Fourier transform infrared (FTIR) spectrometer was used for vibrational characteristics of the synthesized materials. Carbon dioxide adsorption properties of CNMs were determined at various temperatures by Micromeritics ASAP 2020 V3.00 H surface area analyzer, equipped with a water bath.

III. MATERIAL CHARACTERIZATION

A. X-ray diffraction analysis

Structural analyses of CNMs have been carried out by X-ray diffraction pattern. Figure 1 displays the X-ray diffraction patterns of MWNTs and PEMWNTs, which match well with our previous report.[22] A strong signal at ~26° in X-ray diffraction pattern of MWNTs, corresponding to (002) plane, reveals the crystalline nature with 0.34 nm interlayer distance. In addition, signals belonging to (100) and (004) planes are also found at ~43° and ~54°, respectively. Partial oxidation followed by exfoliation-co-reduction highly disturbs the structure of MWNTs. The XRD pattern shows the (002) peak centred at ~26° is merged with a weak signal centred at 24°, corresponding to graphene nanoribbons, which are unraveled from MWNTs due to the rapid exfoliation-co-reduction of oxidized layers.

B. Morphological analysis

Transmission electron microscope images (Figure 2) offer nanoscale morphological information about the carbon nanomaterials. The TEM image of purified MWNTs (Figure 2(a)) confirms the purity, where no amorphous carbon clusters are found. Moreover, it clearly shows the tubular nature of 1D MWNTs, which has distribution of inner (10–20 nm) and outer (30–50 nm) diameters. The inset in Figure 2(a) displays that the ends of MWNTs are open, which facilitates storing CO_2 inside the tubes. MWNTs have SSA of

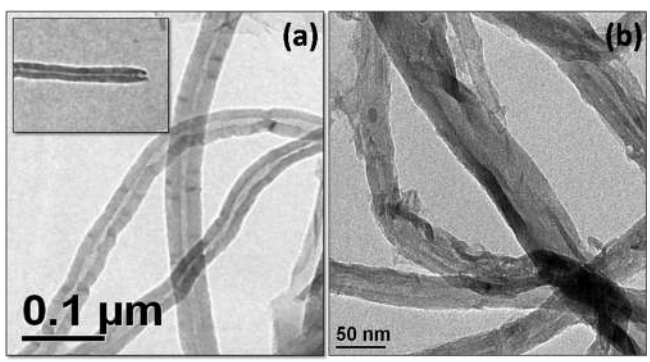

FIG. 2. Transmission electron micrograms of (a) MWNTs and (b) PEMWNTs.

67 $m^2 g^{-1}$ in addition with 0.237 $cm^3 g^{-1}$ of total pore volume and 15.8 nm of average pore width.[22]

Figure 2(a) confirms the partial exfoliation, where unraveled outer layers (graphene nanoribbons) and unaffected inner cylinders are clearly shown. Controlled oxidation followed by the exfoliation-co-reduction selectively unravels the oxidized outer layers of MWNTs. But MWNTs are not cut down since the inner tubes are not affected, which helps to retain the aspect ratio of MWNTs. Hence, PEMWNTs can be viewed as a perfect 1D-2D mixture. As a result, the SSA and total pore volume of this unique structure have been increased to 147 $m^2 g^{-1}$ and 0.398 $cm^3 g^{-1}$, respectively. Nevertheless, the average pore width has been reduced to 12.3 nm, which may be attributed to the introduction of microporosity upon exfoliation.[22]

C. FTIR spectrum analysis

FTIR spectra of purified MWNTs and PEMWNTs are shown in Figure 3. The band corresponding to stretching vibrations of hydroxyl group at ~3450 cm^{-1} is due to the presence of moisture and surface hydroxyl functionalities, which occurs in both materials. The relative intensities of anti-symmetric and symmetric $=CH_2$ vibrations at 2925 and 2855 cm^{-1} are quite strong with PEMWNTs, while they are weak for MWNTs. Purified, non-functionalized MWNTs have least amount of functional groups on the surface, which are resulted from the purification (acid treatment) process. The FTIR spectra of PEMWNTs clearly suggest the presence of large amount of residual $=CH_2$ functional groups even after reduction in hydrogen environment. The stretching vibration of aromatic rings, from the hexagonal honeycomb lattice, has been found at ~1630 cm^{-1} both samples. The peaks at fingerprint region (500–1500 cm^{-1}) can be assigned to the various stretching and bending modes of residual functional groups on PEMWNTs (such as $=CH_2$, -OH, -COOH, >C=O), where most of these signals are absent or weak in the case of MWNTs.[27] Briefly, the bending mode of –OH (1393 cm^{-1}), stretching mode of C-O (1211 cm^{-1}), vibrations of ketone (1058 cm^{-1}) and carboxylic (876 cm^{-1}) groups are much significantly strengthened. These residual functional groups are anticipated to have strong influence in CO_2 adsorption properties of CNMs.

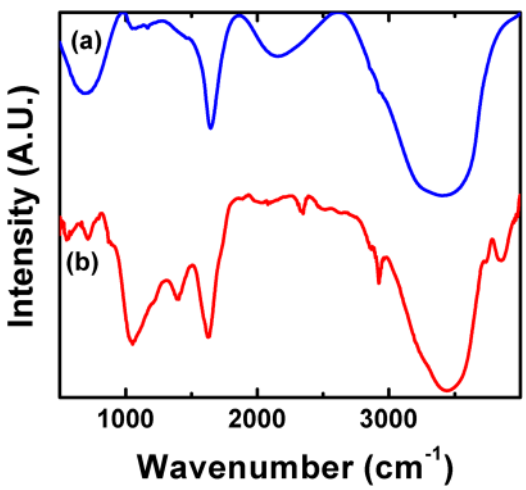

FIG. 3. FTIR spectra of (a) MWNTs and (b) PEMWNTs.

IV. CARBON DIOXIDE ADSORPTION ANALYSIS

A. Analysis procedure

Low pressure carbon dioxide adsorption-desorption studies were carried out using a surface area analyzer (Micromeritics ASAP 2020), which is capable of operating up to 100 kPa pressure. Briefly, mass of a dried sample tube equipped with a seal frit (20 μm pore size) and filling rod was measured (m_1). The sample (150–200 mg) was loaded to the sample tube along with filling rod. The tube was closed by seal frit and connected to the activation port, where the sample tube relies inside a heating mantle.

The sample temperature was raised to 373 K at 10 K min^{-1} and activated for 3 h at this constant temperature under reduced pressure (~7 Pa). The degassed sample tube was weighed (m_2) and the mass difference $m_2 - m_1$ has been taken as the sample mass (m). This method gives accuracy of ±0.001 mg in sample mass. The activated sample cell was equipped with an isothermal jacket and connected into the analysis port.

Available volume inside the sample cell (free space) was calculated using high pure (>99.9%) helium gas at various temperatures of analysis. Here, the sample temperature was maintained constant using thermally insulated water bath along with isothermal jacket. The adsorption-desorption analyses were carried out by vacuum-swing adsorption technique, where the adsorbate was degassed under reduced pressure.

High pure (>99.9%) CO_2 gas was demoisturized by silica gel/P_2O_5 and used throughout the experiments, which has CO and O_2 as possible impurities. In adsorption analysis, known amount (n) of CO_2 gas was allowed into the sample cell. The drop in pressure was continuously recorded until the equilibrium. At equilibrium, the number of moles of gas (n_{eq}) inside the tube has been calculated from the available volume (free space) and sample temperature, using van der Waals equation,

$$\left(P_{eq} + \frac{n^2 a}{V^2}\right)(V - n_{eq} b) = n_{eq} RT, \tag{1}$$

where P_{eq} is the equilibrium pressure corresponding to n_{eq} moles of gas in volume V at temperature T.[28] The difference n-n_{eq} has been reported as adsorbed amount (n_{ad}) in moles at equilibrium. i.e.,

$$n_{ad} = n - n_{eq}. \tag{2}$$

In desorption analysis, the pressure inside the sample cell was reduced by removing known amount of gas (n^*) from the total amount of gas inside the tube ($n = n_{ad} + n_{eq}$). The number of moles of gas (n_{eq}^*) at equilibrium desorption pressure in the known volume (V) was determined by Eq. (1). The amount of CO_2 molecules adsorbed on the surface of adsorbent (n_{ad}^*) was calculated using the equation,

$$n_{ad}^* = n - n^* - n_{eq}^*. \tag{3}$$

The equilibrium specific adsorption capacity (Q_{eq}) has been reported by normalizing the adsorbed amount (n_{ad} or n_{ad}*) to the absolute mass of sample (m). The adsorption isotherms were obtained for both carbon nanostructures up to 100 kPa equilibrium pressure at multiple temperatures.

At low pressures (around 100 kPa), it can be presumed that each adsorption site holds only one adsorbate molecule at pressures far lower than saturation pressures. This adsorption process can be modelled by two isotherm models, known as Langmuir and *Freundlich* adsorption isotherm models. According to Langmuir model, all the adsorption sites have equal energy, but Freundlich model suggests a distribution of adsorption energies. Simulation of these two models with experimental data is expected to suggest the adsorption mechanism.

Langmuir isotherm is represented as,

$$Q_{eq} = \frac{Q_{\max} K_L P}{1 + K_L P}, \tag{4}$$

where Q_{eq} (mol g^{-1}) is the amount of the adsorbed CO_2 molecules at equilibrium pressure P (Pa), Q_{max} (mol g^{-1}) is the maximum adsorption capacity at complete monolayer coverage, and K_L is Langmuir isotherm coefficient.[29]

The surface of carbon nanomaterial is heterogeneous, since it has a distribution of adsorption sites (functional groups and structural defects) with specific adsorption energy. Hence, *Freundlich* adsorption isotherm is expected to model the adsorption process more closely, since it is derived by the integration of Langmuir equation over a heterogeneous surface with well defined energy distribution.

The *Freundlich* equation is,

$$Q_{eq} = K_F P^{\frac{1}{n}}, \tag{5}$$

where Q_{eq} (μmol g^{-1}) is the amount of the adsorbed CO_2 molecules, K_F is Freundlich isotherm constant (μmol g^{-1}), and n is adsorption intensity. K and n are generally temperature dependent constants.[30]

Isosteric heat of adsorption was calculated from the slope of the adsorption isosteres (Van't Hoff plot) at multiple constant adsorbed amounts using Clausius-Clapeyron equation,

$$\Delta H = R\left(\frac{\partial \ln P}{\partial (1/T)}\right)_n, \tag{6}$$

where P is the pressure, T is the temperature of isosteric points on adsorption isotherms, and ΔH is the differential enthalpy of adsorption. The absolute value of ΔH gives the "isosteric heat" of adsorption ($|\Delta H|$). Entropies of adsorption (ΔS) at multiple were obtained from the intercept ($\Delta S/R$) of extrapolated isosteres with *ln P*-axis in Van't Hoff plot.[31]

In vacuum-swing technique, desorption isotherms do not follow the same lend of adsorption, in most of the cases and shows a hysteresis, due to the porosity and surface chemistry of the adsorbent. In order to predict the significance, the hysteresis was quantified by a quantity, called *isothermal adsorbate retention (IAR)*, which is defined as the amount of adsorbate retained when isothermally desorbed at the same pressure. It is mathematically represented as

$$IAR = Q_{des} - Q_{ads}, \tag{7}$$

where Q_{ads} is the equilibrium adsorbate concentration at certain pressure on adsorption isotherm and Q_{des} is the equilibrium adsorbate concentration at the same pressure on desorption isotherm.

B. Equilibration interval determination

Prior to the adsorption experiments, it is important to assign appropriate instrumental parameters to accurately predict the adsorption properties, where the equilibration interval is an important parameter. The equilibrium interval (should not be confused with data acquisition interval) is defined as the time interval between successive pressure readings at certain tolerance. Since the experiments are carried out in sub-ambient pressures and the analyzer has high sensitivity, it is important to set an appropriate equilibration interval.

In this regard, the adsorption analyses on MWNTs were carried out at 298 K with 5, 10, and 20 s equilibration intervals at 2% relative tolerance and 200 Pa absolute tolerance (whichever less is considered at each equilibrium pressure). Figure 4 reveals the maximum adsorption capacity with 10 s equilibrium interval, which is higher than that of 5 s. But, further increase in equilibration interval (20 s) did not show significant improvement in maximum adsorption capacity. Thus, it can be concluded that better data integrity can be achieved with 10 s equilibration intervals.

C. Adsorption isotherm studies

Carbon dioxide adsorption-desorption properties of carbon nanostructures (MWNTs and PEMWNTs) were determined at low pressures (<100 kPa) and at four different temperatures, viz., 283, 288, 293, and 298 K, where the adsorbed amount has been calculated from equilibrium pressure using Eqs. (1)–(3).

The adsorption isotherms of MWNTs (Figure 5(a)) show almost straight line behavior till 100 kPa and the experimental data could not be fitted to Langmuir equation (Table

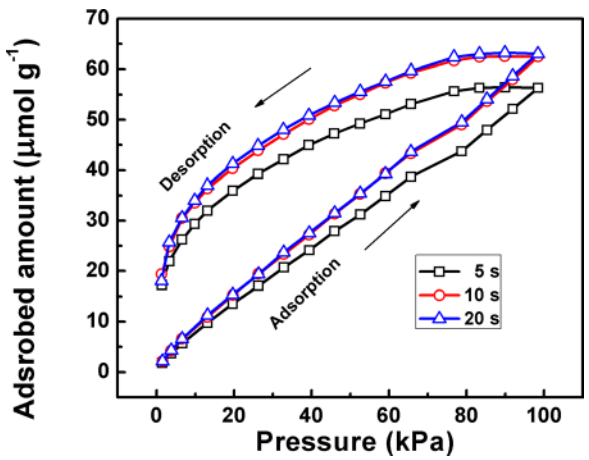

FIG. 4. CO_2 adsorption-desorption isotherms of MWNTs at different equilibration intervals at 2% relative pressure tolerance and 200 Pa absolute pressure tolerance and 298 K sample temperature.

I). This suggests that the gas molecules are not simply adsorbed on MWNTs surface sites. Matranga *et al*. have identified the trapping of CO_2 molecules in the interstitial sites of carbon nanotubes.[32,33] Here, MWNTs have average pore size of ~15 nm with 0.232 $cm^3 g^{-1}$ specific pore volume, which traps CO_2 molecules inside the inner tubes and interstitials. But, the isotherms fit better with Freundlich model, where trapping pores are more affine sites in the distribution.

It has to be noted that the value of n is close to unity, suggesting that the adsorption follows linear isotherm. Here, trapping CO_2 inside MWNTs is relatively energetic with high capacity. Hence, the equilibrium may be attained at high pressures. MWNTs adsorb 88 μmol g^{-1} at 283 K, which decreases with increase in temperature to 63 μmol g^{-1} at 298 K. Mishra *et al*. have reported 14.3 mmol g^{-1} of Q_{eq} for the MWNTs, at 1200 kPa and room temperature.[34] This is much higher than the extrapolated value of single layer adsorption (~0.5 mmol g^{-1}), obtained in this study. It is possible only when CO_2 molecules are condensed inside the tubes as suggested by the literature.[35] The Q_{eq} value decreases with increase in temperature, which can be imputed to the increase in kinetic energy of CO_2 molecules with temperatures. This helps the molecules to escape from surface active sites and pores.

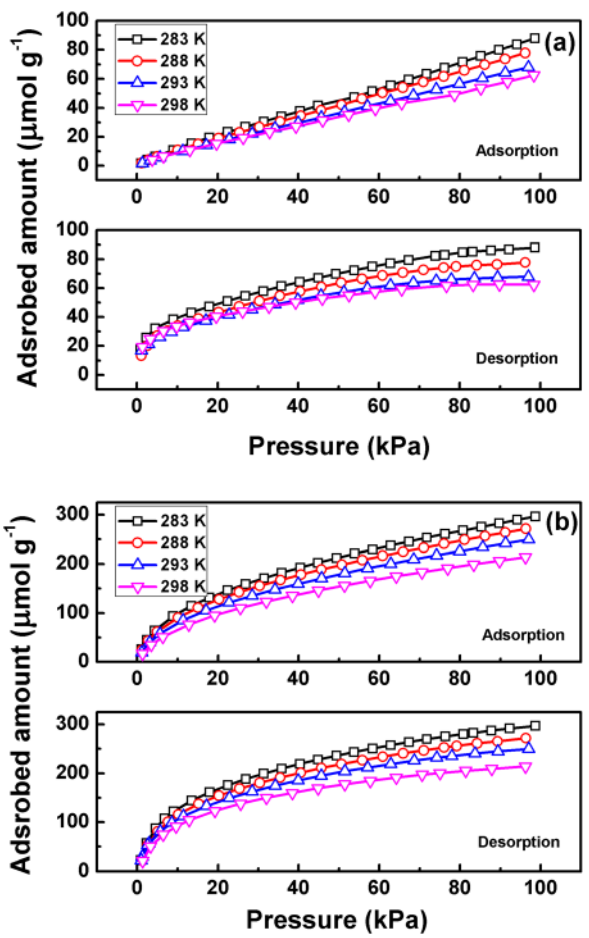

FIG. 5. CO_2 adsorption-desorption isotherms of (a) MWNTs and (b) PEMWNTs at multiple sample temperatures.

Carbon dioxide adsorption-desorption isotherm studies on PEMWNTs are also carried out at multiple temperatures (Figure 5(b)), and the equilibrium adsorbed amounts at ~100 kPa are given in Table I. These values clearly show that the adsorption capacity attains nearly 4-fold improvement upon partial exfoliation. As discussed earlier, the SSA of PEMWNTs (147 $m^2 g^{-1}$) is higher than MWNTs (67 $m^2 g^{-1}$). This can be certainly correlated with the adsorption capacity. The temperature dependency of adsorption on PEMWNTs follows that of MWNTs. Although the unaffected inner core tubes trap CO_2 molecule, the contribution from physisorption at outer surface is maximum, which suppresses the characteristics of trapped CO_2 inside the tubes in adsorption-desorption isotherms.

Adsorption isotherm fits better with Freundlich model ($R^2 = 0.999$) than Langmuir model ($R^2 = 0.98$). The initial adsorption rate (from K_L) would be improved due to the residual surface functional groups, which decrease with increase in temperature, indicating the temperature dependant surface affinity towards adsorbate. The n values of Freundlich isotherm for PEMWNTs are double that of MWNTs. This indicated the favorability of adsorption on PEMWNTs surfaces.[36]

Adsorption occurs when the interaction between the molecular orbital of adsorbate and adsorbent surface reaches a lowest energy configuration (i.e., most stable state). Furuya *et al*. obtained a linear relationship (inversely proportional) between HOMO (*highest occupied molecular orbital*) density and the experimentally determined Freundlich coefficient $1/n$ by molecular modeling of adsorption, which implies that electron density of both adsorbates and adsorbents is one of the major factors determining the adsorption properties.[37]

It is interesting to see in the present study that PEMWNTs has almost half the $1/n$ value of MWNTs, suggesting high HOMO density. This may be attributed to the presence of residual carboxyl, hydroxyl, and carbonyl functional groups and structural defects. Briefly, the oxygen containing functional groups, such as hydroxyl and carbonyl, raises the HOMO level by the fact that electron density injected from oxygen into the carbon hexagonal lattice traps the electronic cloud at localized sites, which increases the strength of adsorption sites.[38] On the other hand, structural defects trap excess electron around the defect site, which produces localized LUMO and delocalized HOMO in the carbon lattice.[39]

Freundlich coefficient K_F, by means of K_F/n, gives the information about the molecular orbital energy of adsorbate and adsorbent system, i.e., adsorption energy. PEMWNTs show higher K_F/n value than that of MWNTs, which is expected to reflect in isosteric heat of adsorption.

D. Isothermal adsorbate retention

The desorption isotherms are unique for MWNTs and show large hysteresis. This hysteresis may be attributed to the CO_2 trapping in MWNTs as discussed earlier. The IAR value of MWNTs as a function of equilibrium pressure at multiple temperatures is shown in Figure 6(a). MWNTs

TABLE I. Adsorption isotherm fitting parameters. Units: Q_{eq} (μmol/g^{-1}), Q_{max} (μmol/g^{-1}), K_L (k Pa^{-1}), n (a.u.), and K_F (μmol g^{-1} k Pa$^{-(1/n)}$).

			Langmuir			Freundlich		
Material	Temperature (K)	Q_{eq} at 100 kPa	Q_{max}	K_L	R^2	$1/n$	K_F	R^2
MWNTs	283	88		Fit did not converge		0.912	1.305	0.998
	288	78				0.909	1.207	0.999
	293	68				0.912	1.038	0.999
	298	63				0.871	1.123	0.998
PEMWNTs	283	297	387	0.0270	0.979	0.483	32.184	0.999
	288	271	357	0.0269	0.981	0.491	28.763	0.999
	293	250	338	0.0245	0.983	0.508	24.407	0.999
	298	214	292	0.0242	0.986	0.517	20.306	0.998

show 23 μmol g^{-1} IAR at 50 kPa desorption pressure and at 283 K sample temperature, while that becomes 21 μmol g^{-1} at 298 K. Generally, the amount of retention reduces significantly at high temperatures, since the CO_2 molecules attain high kinetic energy at high temperatures, which helps them to escape from the surface.

The molecules adsorbed inside the MWNTs have higher binding energy than those on the outer surface.[13] At low pressures, IAR falls rapidly due to the rapid desorption of trapped CO_2 molecules. However, the adsorbate molecules are not completely desorbed even at near-zero pressures. This can be imputed to the permanent trapping of CO_2 molecules inside MWNTs and the interstitials.[33] From desorption isotherm and IAR, it can be concluded that CO_2 molecules are trapped inside MWNTs with high binding energy.

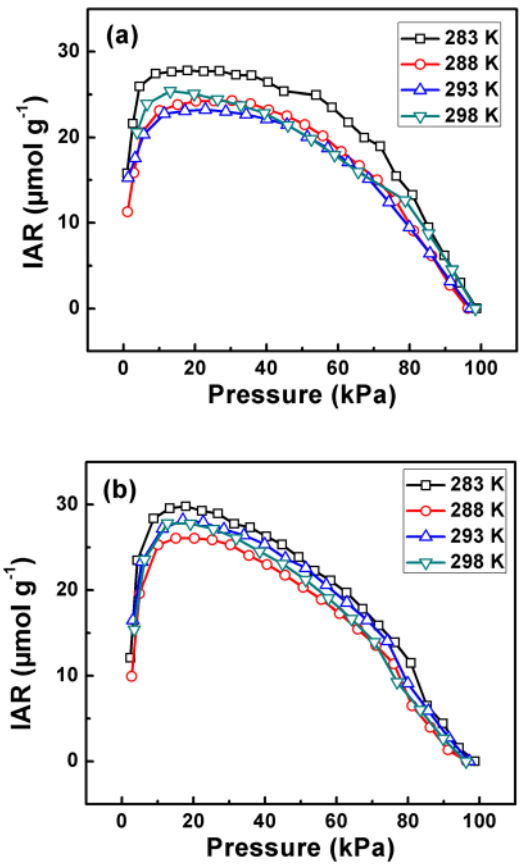

FIG. 6. Isothermal adsorbate retention of (a) MWNTs and (b) PEMWNTs as a function of equilibrium pressure.

Surprisingly, the adsorbate retention of PEMWNTs (Figure 6(b)) is almost equal to that of MWNTs, viz. 27 and 23 μmol g^{-1} at 283 and 298 K at 50 kPa desorption pressure, respectively. Here, the volume inside the MWNTs is not affected by partial exfoliation, which leads to unchanged adsorbate retention. This phenomenon strongly suggests that the CO_2 molecules are reversibly adsorbed on the distributed surface adsorption sites. The amount of permanently stored CO_2 can be predicted directly from the low pressure IAR value at very low pressures (<1 kPa). This value is almost same for both PEMWNTs (10 μmol g^{-1}) and MWNTs (13 μmol g^{-1}) at 298 K.

E. Areal adsorption capacity (AAC)

The discussions on isotherms reveal that the adsorption capacity is proportional to the surface area. However, in general the adsorption capacity strongly depends on the affinity (or the surface chemistry) of adsorbent with the adsorbate molecules. Moreover, the porosity of the adsorbent is also expected to play a major role in adsorption capacity. In order to understand this phenomenon, the AACs (adsorption per unit surface area) of the studied adsorbents have been determined at different temperatures (Figure 7). PEMWNTs show the higher AAC (2.02 μmol m^{-2}) than MWNTs (1.31 μmol m^{-2}) at 283 K sample temperature due to the large amount of residual functional groups.[19] Upon partial exfoliation, the surface area and pore volume of MWNTs are increased by 2.19 and 1.7 times, respectively. But the adsorption capacity at 298 K is

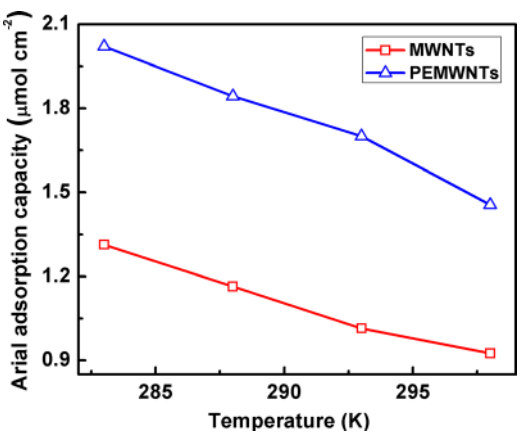

FIG. 7. Areal adsorption capacity of MWNTs and PEMWNTs at 283, 288, 293, and 298 K sample temperatures.

improved by 3.4 times, i.e., improvement in adsorption capacity is not in the rate at which surface area and pore volume increase. This can be attributed to the presence of residual surface functional groups, as predicted by FTIR analysis. Hence, it can be concluded that surface chemistry influences equally that of lateral surface properties, such as surface area and pore volume in adsorption capacity.

Although PEMWNTs show improved AAC due to large amount of residual functional groups, its IAR is not increased. This suggests that the CO_2 molecules interact with surface anchoring sites (functional groups and structural defects) reversibly, while it is trapped inside the tubes with high energy.

F. Thermodynamic parameters of adsorption

The isosteric heat of adsorption ($|\Delta H|$) represents the strength of adsorbate–adsorbent interaction, which is defined as the difference between the activation energies for adsorption and desorption. The adsorption isosteres of CO_2 adsorption on MWNTs and PEMWNTs are shown in Figure 8. All these isosteres follow Arrhenius relation with negative slope, suggesting the temperature-dependent adsorption rate, which decreases with increasing temperature (physisorption is exothermic). Here, $|\Delta H|$ was calculated from the slope of adsorption isosteres (Figure 8) at multiple adsorbed amounts, using Eq. (6).

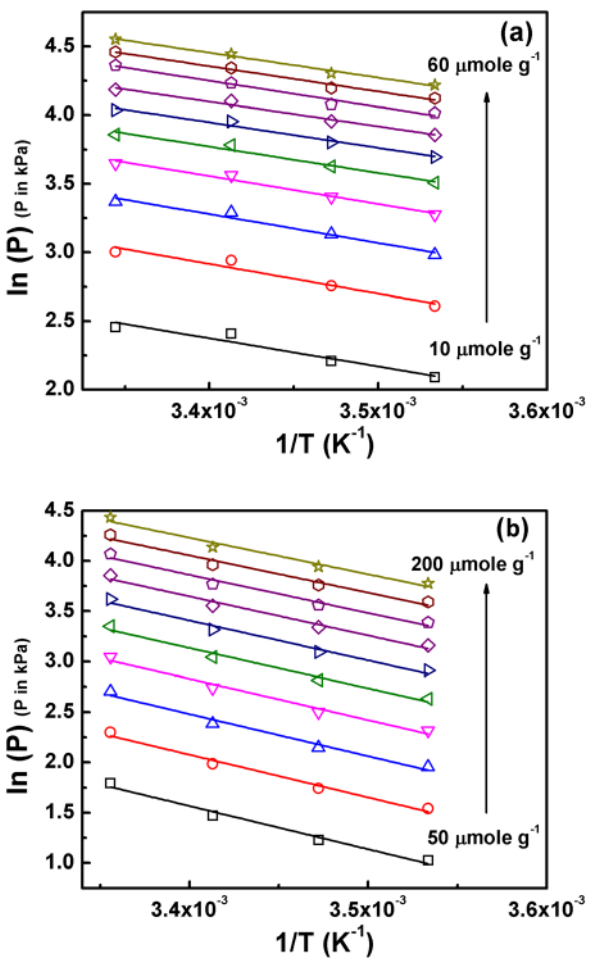

FIG. 8. CO_2 adsorption isosteres (van't Hoff plot) of (a) MWNTs and (b) PEMWNTs with different adsorbed amount.

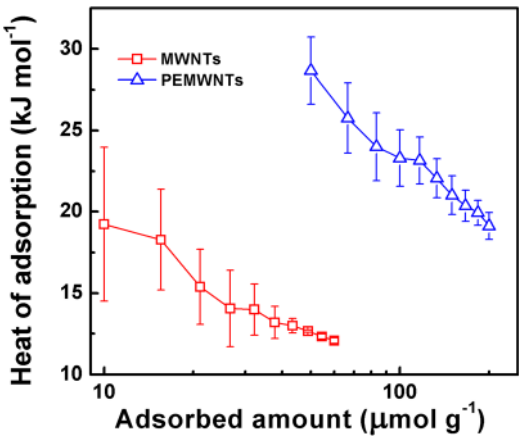

FIG. 9. Comparison of isosteric heats of adsorption of MWNTs and PEMWNTs as a function of adsorbed amount.

The isosteres with low adsorbed amounts result in a large uncertainty in heat of adsorption, particularly with MWNTs, which stems from the fact that the uncertainty is high at low adsorbed amount. Hence, $|\Delta H|$ values are reported at the maximum adsorbed amount. MWNTs show $12.1 \pm 0.2\,\mathrm{kJ\,mol^{-1}}$ at $60\,\mu\mathrm{mol\,g^{-1}}$ of adsorbed amount (Figure 8(a)). This is in close agreement with Hsu *et al.*, who reported similar values at high pressures.[12] The theoretical prediction on heat of adsorption of CO_2 on MWNTs system also shows a similar value for unrestricted adsorption in the inner and outer surfaces.[13]

The heat of adsorption of CO_2 on PEMWNTs surface is $19.1 \pm 0.8\,\mathrm{kJ\ mol^{-1}}$ at $200\,\mu\mathrm{mol\ g^{-1}}$ adsorbed amount (Figure 8(b)). This is significantly higher than that observed with MWNTs, which is in close agreement with the Freundlich isotherm analysis, where molecular orbital energy of adsorbate and adsorbent system is higher for PEMWNTs sorbent. Here, the adsorbate-adsorbent interaction is improved by residual functional groups and surface defects as discussed in areal adsorption capacity.

The variation in heat of adsorption upon surface coverage has been determined from adsorption isosteres of carbon nanomaterials at various adsorbed amounts and presented in Figure 9. For both adsorbents, the $|\Delta H|$ value gradually decreases with increase in surface coverage. This implies

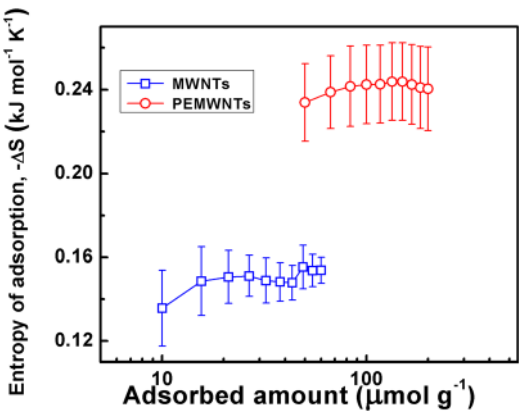

FIG. 10. Comparison of entropy change in adsorption of CO_2 on MWNTs and PEMWNTs as a function of adsorbed amount.

that initially CO_2 molecules are attracted by the high affinity sites such as trapping pores, groove structures, and functional groups. As the CO_2 molecules are supplied continuously, the high affinity sites are saturated and the adsorption is continued by the low energy pores. The high-energy narrow pores are filled only at high pressures or are even inaccessible to the CO_2 molecules. Further addition of CO_2 molecules may be loosely bound on the surface with low binding energy and are mobile on the surface.

The entropy changes caused by adsorption of CO_2 ($-\Delta S$) were calculated from the van't Hoff plot, where the intercepts with *ln P*-axis give $\Delta S/R$ value at different adsorbed amount. Figure 10 shows quite consistent values of entropy over the range of adsorbed amount. It can be seen that the average ΔS values of -0.149 ± 0.009 and -0.24 ± 0.02 kJ mol^{-1} K^{-1} are for MWNTs and PEMWNTs, respectively. This is almost one order higher than the reported value for activated carbon.[11]

V. CONCLUSION

Investigation of carbon dioxide adsorption-desorption properties of MWNTs (1D) and PEMWNTs (1D + 2D)) studied at low pressure (<100 kPa) revealed that MWNTs have unique adsorption-desorption properties due to the 1D tubular nature and possible CO_2 trapping in the tubes and interstitials. The adsorption capacity of PEMWNTs is higher than that of MWNTs indicating clearly that the surface area of adsorbent is one of the major factors deciding the adsorption capacity. Moreover, the surface affinity influences the adsorption capacity much significantly. The isothermal adsorbate retention is not changed much upon partial exfoliation. The areal adsorption capacity of PEMWNTs is higher than that of MWNTs due to the presence of residual functional groups and structural defects. Storage of CO_2 inside the inner tubes and interstitials is more energetic; while at the surface sites are reversible. Isosteric heat of adsorption is in physisorption range for both materials, but PEMWNTs have relatively higher value than that of MWNTs. The changes in entropies upon adsorption of CO_2 on these carbon nanomaterials are higher than that reported for activated carbon.

ACKNOWLEDGMENTS

The authors acknowledge SAIF-IITM for FTIR analysis. One of the authors (P. Tamilarasan) acknowledges Indian Institute of Technology Madras (IITM) for the financial supports (senior research fellowship).

[1]Q. Wang, J. Luo, Z. Zhong, and A. Borgna, Energy Environ. Sci. **4**, 42 (2011).
[2]S. Choi, J. H. Drese, and C. W. Jones, ChemSusChem **2**, 796 (2009).
[3]P. Tamilarasan and S. Ramaprabhu, Int. J. Greenhouse Gas Control **10**, 486 (2012).
[4]A. K. Mishra and S. Ramaprabhu, AIP Adv. **1**, 032152 (2011).
[5]J. D. Baniecki, M. Ishii, K. Kurihara, K. Yamanaka, T. Yano, K. Shinozaki, T. Imada, and Y. Kobayashi, J. Appl. Phys. **106**, 054109 (2009).
[6]A. D. K. Jones, T. Bekkedahl, and C. Kiang, Nature **386**, 377 (1997).
[7]A. K. Mishra and S. Ramaprabhu, J. Appl. Phys. **116**, 064306 (2014).
[8]P. Tamilarasan, T. S. Remya, and S. Ramaprabhu, Graphene **1**, 3 (2013).
[9]A. Kumar Mishra and S. Ramaprabhu, RSC Adv. **2**, 1746 (2012).
[10]V. R. Deitz, J. Phys. Chem. **71**, 830 (1967).
[11]B. Guo, L. Chang, and K. Xie, J. Nat. Gas Chem. **15**, 223 (2006).
[12]S.-C. Hsu, C. Lu, F. Su, W. Zeng, and W. Chen, Chem. Eng. Sci. **65**, 1354 (2010).
[13]M. Rahimi, J. K. Singh, D. J. Babu, J. J. Schneider, and F. Müller-Plathe, J. Phys. Chem. C **117**, 13492 (2013).
[14]M. Bienfait, P. Zeppenfeld, N. Dupont-Pavlovsky, M. Muris, M. R. Johnson, T. Wilson, M. DePies, and O. E. Vilches, Phys. Rev. B **70**, 035410 (2004).
[15]Z. Jijun, B. Alper, H. Jie, and L. Jian Ping, Nanotechnology **13**, 195 (2002).
[16]J. Li, X. Cheng, J. Sun, C. Brand, A. Shashurin, M. Reeves, and M. Keidar, J. Appl. Phys. **115**(16), 164301 (2014).
[17]S. S. Jyothirmayee Aravind and S. Ramaprabhu, J. Appl. Phys. **112**, 124304 (2012).
[18]M. S. Shafeeyan, W. M. A. W. Daud, A. Houshmand, and A. Shamiri, J. Anal. Appl. Pyrolysis **89**, 143 (2010).
[19]S. Khalili, A. A. Ghoreyshi, and M. Jahanshahi, Chem. Ind. Chem. Eng. Q. **19**, 153 (2013).
[20]H. Wang, Y. Wang, Z. Hu, and X. Wang, ACS Appl. Mater. Interfaces **4**, 6827 (2012).
[21]H. Zhao, W. Xu, L. Song, Q. Mei, C. Chen, L. Miao, and J. Jiang, J. Appl. Phys. **112**, 074316 (2012).
[22]P. Tamilarasan and S. Ramaprabhu, J. Mater. Chem. A **2**, 14054 (2014).
[23]M. Shaijumon and S. Ramaprabhu, Chem. Phys. Lett. **374**, 513 (2003).
[24]W. S. Hummers and R. E. Offeman, J. Am. Chem. Soc. **80**, 1339 (1958).
[25]N. L. Rangel, J. C. Sotelo, and J. M. Seminario, J. Chem. Phys. **131**, 031105 (2009).
[26]A. Kaniyoor, T. T. Baby, and S. Ramaprabhu, J. Mater. Chem. **20**, 8467 (2010).
[27]N. Colthup, J. Opt. Soc. Am. **40**, 397 (1950).
[28]J. D. Van Der Waals, *On the Continuity of the Gaseous and Liquid States* (Courier Dover Publications, 2004).
[29]I. Langmuir, J. Am. Chem. Soc. **38**, 2221 (1916).
[30]H. Freundlich, *Kapillarchemie: eine Darstellung der Chemie der Kolloide und verwandter Gebiete* (Akademische verlagsgesellschaft mbh, 1922).
[31]W. Gao, D. Butler, and D. L. Tomasko, Langmuir **20**, 8083 (2004).
[32]C. Matranga, L. Chen, M. Smith, E. Bittner, J. K. Johnson, and B. Bockrath, J. Phys. Chem. B **107**, 12930 (2003).
[33]C. Matranga and B. Bockrath, J. Phys. Chem. B **108**, 6170 (2004).
[34]A. K. Mishra and S. Ramaprabhu, Energy Environ. Sci. **4**, 889 (2011).
[35]R. I. Masel, *Principles of Adsorption and Reaction on Solid Surfaces* (Wiley, 1996).
[36]Y. Otake, N. Kalili, T. H. Chang, and E. Furuya, Sep. Purif. Technol. **39**, 67 (2004).
[37]E. G. Furuya, H. T. Chang, Y. Miura, and K. E. Noll, Sep. Purif. Technol. **11**, 69 (1997).
[38]A. Chutia, F. Cimpoesu, H. Tsuboi, and A. Miyamoto, Chem. Phys. Lett. **503**, 91 (2011).
[39]H. Tachikawa and H. Kawabata, J. Phys. Chem. C **113**, 7603 (2009).